Finestructure of Wind Waves Analyzed with Wavelet Transform

ZHENG SHEN, WEI WANG, AND LIMING MEI

Institute of Physical Oceanography, Ocean University of Qingdao, Qingdao, People's Republic of China

12 May 1992 and 29 September 1993

ABSTRACT

One central problem in the study of wind-generated gravity waves is the energy balancing process in the equilibrium spectral subrange. In considering the predicted equilibrium spectral forms from physical models proposed by Kitaigorodskii, other investigators accepted that the statistical equilibrium state is effectively characterized by the wave action conservation law: $\partial E/\partial t + \vec{C}_g \cdot \nabla E = 0$, where E is the wave energy spectrum and $\vec{C}_g = \nabla_k \omega(k)$ is the group velocity. Here the continuous wavelet transform is used to analyze typical sets of wind-generated gravity wave data obtained both in the ocean and in a wind–wave channel. This "space scale" analysis is shown to provide the first visual evidence that when the fetch is not very short, the wave action conservation law mentioned above is not convenient to describe the dynamics of the wave components in the equilibrium range estimated from its energy spectrum.

1. Introduction

The mechanisms involved in wind-generated gravity waves have been the subject of intensive theoretical and experimental investigation over the last three decades. According to the current status of our understanding, the random character of wind waves can be effectively approached by a stationary, ergodic random process. Wind waves, being dominated by strong gravitational restoration, are weakly nonlinear with wind forcing, wave breaking, and the interaction among different scales as the associated control terms.

The common model for the surface elevation $\zeta(\mathbf{x}, t)$, initiated by Longuet-Higgins (1957), assumes

$$\zeta(\mathbf{x}, t) = \sum_{n=1}^{\infty} a_n \cos(\mathbf{k}_n \cdot \mathbf{x} + \omega_n t + \phi_n), \quad (1.1)$$

where ϕ_n is uniformly distributed between 0 and 2π and the a_n, $\mathbf{k}_n$, and ω_n are considered to be fixed for all realizations. The a_n are constrained such that

$$\sum_{\mathbf{k}}^{\mathbf{k}+\delta\mathbf{k}} \sum_{\omega}^{\omega+\delta\omega} \frac{1}{2} a_n^2 = E(\mathbf{k}, \omega)\delta\mathbf{k}\delta\omega, \quad (1.2)$$

where $E(\mathbf{k}, \omega)$ is the Fourier wave spectrum. The directional frequency spectrum is defined as

$$G(\omega, \theta) = 2\int_0^{\infty} E(\mathbf{k}, \omega) k dk, \quad (1.3)$$

where θ is the angle between the wind direction and the wavenumber vector. The frequency spectrum is defined as

$$S(\omega) = \int_{-\pi}^{\pi} G(\omega, \theta) d\theta. \quad (1.4)$$

The evolution of the directional frequency spectrum $G(\omega, \theta, \mathbf{x}, t)$ was described by Hasselman and others (see, e.g., Khandekar 1989), based on the wave action conservation law

$$\frac{DG}{Dt} = \frac{\partial G}{\partial t} + \vec{C}_g \cdot \nabla G = S_{in} + S_{nl} + S_{ds}. \quad (1.5)$$

Here S_{in}, S_{nl}, and S_{ds} are the source terms representing the spectral distributions of wind input, the transfer of energy associated with nonlinear wave–wave interactions, and the energy dissipation through wave breaking and turbulence; $\vec{C}_g$ is the group velocity of the wave field

$$\vec{C}_g = \nabla_k \omega(k) = \frac{g}{2\omega} \frac{\mathbf{k}}{k}. \quad (1.6)$$

This spectral approach of the wind waves has proven to be successful in diverse fields, such as practical wave forecasting and the engineering design of marine structures and vehicles. But when we use the wave spectra to describe the finestructure of wind wave surfaces, we find that our knowledge of the wind wave spectra is incomplete. Interest in this problem has been heightened in recent years by the fundamental role of short surface wave components in active microwave remote sensing of the oceans. The two following questions seem to be fundamental. First, can $\zeta(\mathbf{x}, t)$ be ap-

Corresponding author address: Dr. Zheng Shen, Institute of Physical Oceanography, Ocean University of Qingdao, Qingdao, 266003, People's Republic of China.

proached effectively by a superposition of infinitesimal trigonometric wave components? Second, does the energy of the short wave components propagate at the group velocity $\tilde{C}_g$?

In this paper our investigation is of the surface elevation $\zeta(t)$. Wind waves in nature, instead of being permanently superposed by free infinitesimal trigonometric wave components, experience continuously the turbulent wind forcing, wave breaking, and energy exchange between different scales. These three processes may well result in localized singularities in $\zeta(t)$. In such cases, when applying a Fourier transform to $\zeta(t)$, these localized singularities will be completely delocalized throughout the frequency spectrum $S(\omega)$. If this singularity contribution to $S(\omega)$ is significant, we will lose the essential information of $\zeta(t)$ in describing wind waves by the Longuet-Higgins spectral model Eqs. (1.1) and (1.2).

The singularities in $\zeta(t)$ can be visualized by the continuous wavelet transform, which is a mathematical technique introduced in the early 1980s in the context of seismic data analysis (Goupillaud et al. 1984). The wavelet analysis provides a two-dimensional unfolding of one-dimensional signals, resolving both position and scale as independent variables. It has been shown that the continuous wavelet transform is well adapted for investigating the coherent structures in turbulent flows (Farge 1992). In the present paper, wind-generated gravity waves are analyzed with a continuous wavelet transform, which is introduced in the following section. It is shown that there are isolated singularities in $\zeta(t)$. They make a significant contribution to the observed Fourier frequency spectra, especially in the high frequency range. The results give some new viewpoints concerning our understanding of wind waves and suggest that the spectral model Eqs. (1.1), (1.2), and (1.5) are not suitable for describing the dynamics of short wave components of $\zeta(t)$ when the wind fetch is long.

2. Wavelet transform

We introduce here the continuous wavelet transform of a real function over a real line R. We limit this study to the basic facts used in the following; for more detailed information see Grossmann and Morlet (1987) and Farge (1992).

The continuous wavelet transform of a real signal $\zeta(t)$ with respect to the analyzing wavelet $g(t)$ [in general, $g(t)$ is complex] is defined as the function:

$$\tilde{\zeta}(\tau, T) = \frac{1}{\sqrt{T}} \int_{-\infty}^{+\infty} g^*\left(\frac{t-\tau}{T}\right)\zeta(t)dt, \quad (2.1)$$

where $T \in R^+$ is the scale dilation parameter corresponding to the width of the wavelet, $\tau \in R$ is the translation parameter corresponding to the position of the wavelet, and g^* denotes the complex conjugate of g. The wavelet $g(\in L^2 \cap L^1)$ satisfies the following admissible condition:

$$C_g = 2\pi \int_{-\infty}^{+\infty} |\hat{g}(\omega)|^2 \frac{d\omega}{|\omega|} < +\infty, \quad (2.2)$$

where $\hat{g}(\omega)$ is the Fourier transform of $g(t)$; that is,

$$\hat{g}(\omega) = \frac{1}{2\pi} \int_{-\infty}^{+\infty} g(t)e^{-i\omega t}dt. \quad (2.3)$$

If $\hat{g}(\omega) = 0$ for $\omega < 0$, we shall say that $g(t)$ is a progressive wavelet. Expressing Eq. (2.1) in terms of Fourier transforms, one gets

$$\tilde{\zeta}(\tau, T) = 2\pi\sqrt{T} \int_{-\infty}^{+\infty} \hat{\zeta}(\omega)\hat{g}^*(T\omega)e^{i\tau\omega}d\omega. \quad (2.4)$$

The wavelet transform (2.1) is a sort of a mathematical microscope, whose magnification is $1/T$, whose position is τ, and whose optics is given by the choice of the specific wavelet g.

In this paper, the analyzed wavelet is chosen as

$$g(t) = e^{(-t^2/2+i2\pi t)}. \quad (2.5)$$

This is the "standard Morlet wavelet," which has been used extensively. As shown in Fig. 2, the standard Morlet wavelet is a plane wave of frequency $\omega_g = 2\pi$, modulated by a Gaussian envelope of unit width. In Fourier space, the standard Morlet wavelet is given by

$$\hat{g}(\omega) = \frac{1}{\sqrt{2\pi}} e^{-(\omega-2\pi)^2/2}. \quad (2.6)$$

For all practical purposes, the Morlet wavelet is admissible and progressive.

It has been proven that the information contained in the wavelet coefficients is redundant and there are many different reconstruction formulas, of which we write down the most simple one:

$$\zeta(t) = C_\delta^{-1} \int_{0^+}^{+\infty} \tilde{\zeta}(\tau, T) \frac{dT}{T^{3/2}}, \quad (2.7)$$

with

$$C_\delta = \sqrt{2\pi} \int_{-\infty}^{+\infty} \hat{g}(\omega) \frac{d\omega}{|\omega|}.$$

Now we list some of the main properties of the wavelet transform. We denote the continuous wavelet transform of a function $\zeta(t)$ by the operator notation $W[\zeta](t)$ and the resulting wavelet coefficients by $\tilde{\zeta}(\tau, T)$.

A very simple but fundamental property of the continuous wavelet transform is its covariance with respect to translations and dilations of the signal; namely,

$$W[\zeta](t - t_0) = \tilde{\zeta}(\tau - t_0, T), \quad (2.8)$$

$$W[\zeta](T_0 t) = T_0^{-1}\tilde{\zeta}(T_0\tau, T_0 T). \quad (2.9)$$

The covariance of translation (2.8) has an immediate consequence. It can be shown that the frequency of a monochromatic signal can be obtained from the phase

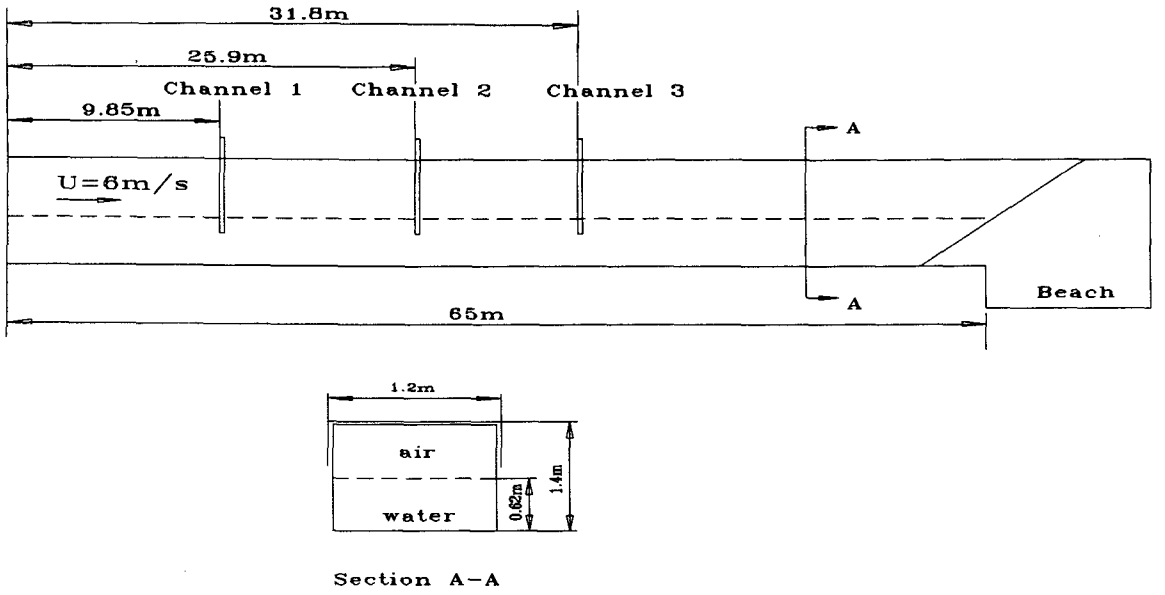

FIG. 1. Plan of the wind wave channel.

of any restriction of its wavelet transform to a horizontal line T = const. Let $f(t)$ be a function that is continuous, not necessarily differentiable in t_0, such that

$$|f(t + t_0) - f(t)| = c|t|^{\alpha} \qquad (2.10)$$

with $\alpha < 1$ and constant $c > 0$. Then in the neighborhood of $\tau = t_0$, it is easily verified from the covariance of dilation (2.9):

$$\tilde{f}(T_0\tau, T_0T) = T_0^{1+\alpha}\tilde{f}(\tau, T) \qquad (2.11)$$

with $T_0 \in R^+$. This implies that the wavelet transform of a homogenous signal is fully determined by its restriction to any line T = const. It can also be proved that the following estimate of $\tilde{f}(t_0, T)$ is valid:

$$\tilde{f}(t_0, T) \sim ce^{i\phi}T^{\alpha+1/2} \qquad (2.12)$$

for $T \to 0$, where ϕ is the phase of the wavelet coefficients. Equations (2.11) and (2.12) will be used in the following section to test singularities categorized by Eq. (2.10) in wind wave datasets.

The effective width, σ_* say, of the standard Morlet wavelet (2.5) is a limited value ($\sigma_* \approx 4.$), as shown in Fig. 2. Hence it can be verified from Eq. (2.1) that the wavelet coefficients corresponding to the position t_0 will all be contained in the influence cone in the wavelet space:

$$\tau \in [t_0 - T\sigma_*/2, t_0 + T\sigma_*/2]. \qquad (2.13)$$

Similarly, on account of the fact that the effective widths of Eqs. (2.5) and (2.6) are identical, the wavelet coefficients corresponding to the scale T_0 will only be contained in the subband defined by

$$T \in \left[T_0 - \frac{T_0\sigma_*}{4\pi + \sigma_*}, T_0 + \frac{T_0\sigma_*}{4\pi - \sigma_*}\right]. \qquad (2.14)$$

Another property of the continuous wavelet transform is that it conserves the energy of the signal:

$$\int_{-\infty}^{+\infty} |\zeta(t)|^2 dt = c_g^{-1} \int_{0^+}^{+\infty} \int_{-\infty}^{+\infty} \tilde{\zeta}(\tau, T)\tilde{\zeta}^*(\tau, T) \frac{d\tau dT}{T^2}. \qquad (2.15)$$

It implies that there is no loss of information in transforming the signal into its wavelet coefficients. In fact, the energy conservation is not only true globally, but also locally if one considers all coefficients inside the influence cone (2.13) and (2.14).

3. Experimental results using wavelet

The wave data used in the present paper were obtained from both laboratory simulations and sea field observations. The laboratory data measured by a capacitance wave gauge and a resistance wave gauge in the laboratory wind wave channel (Fig. 1) are listed in Table 1. The field observations were performed at an oil platform (39°15′N, 119°50′E) located in the Bohai Sea, which is semiclosed and connected with the Yellow Sea through a strait. Only waves generated by offshore winds are considered. The Bahai Sea bottom is flat and shoals to the shoreline at a gentle slope. Waves grow while propagating from shore to the platform where the depth is 27 m, so the waves may be considered as being generated in deep water. Details of these observations are summarized in Table 1.

The selected wave data satisfy the following criteria: 1) Waves are generated by an approximately constant wind of long duration (>1.5 h in the field and >10 min in the laboratory); 2) dominant swells do not coexist with wind waves; and 3) wave frequency spectra (estimated by standard numerical methods) are of a single peaked form.

Figures 3a and 4a show typical examples of the three-dimensional display of the modulus of the wavelet transform Eq. (2.1), that is, $|\tilde{\zeta}(\tau, T)|$. Figure 3a is calculated from laboratory dataset 2; only a small section of it is shown. Figure 4a is calculated from field dataset 4. The two corresponding water surface elevation datasets are plotted in Figs. 3b and 4b. It is found that amplitudes of the wave components at high frequencies (corresponding to small T) are remarkably inhomogeneous, with very sharp peaks sporadically distributed along the time axis τ. As noted in section 2, being different from a Fourier transform, the information contained in the wavelet coefficients is redundant. The value of $|\tilde{\zeta}(\tau_0, T_0)|$ cannot be absolutely interpreted as the amplitude of the wave component of $\omega = 2\pi/T_0$ at $t = \tau_0$. Here $\tilde{\zeta}(\tau_0, T_0)$ is only local in the influence cone specified by Eqs. (2.13) and (2.14). At high frequencies, the distances between the sharp peaks along the τ axis in Figs. 3a and 4a are at least five times larger than the width of the influence cone (2.13), $T\sigma_*$. Hence we can interpret the inhomogeneity of the modulus of the wavelet coefficients along the τ axis at high frequencies as the inhomogeneity of the high-frequency wave components of $\zeta(t)$. A common pitfall in decoding the wavelet coefficients is emanated from Eq. (2.4): it seems that the wavelet transform was only a filter operating on the signal, so the behavior of the wavelet coefficients should appear as a wave group. From Eqs. (2.4) and (2.14), it is easy to verify that the effective width of $\tilde{g}(T_0\omega)$ is

$$\Delta\omega = \frac{\omega_0\sigma_*}{2\pi} \tag{3.1}$$

TABLE 1. Field and laboratory wind wave data details.

Dataset	Date	Time (GMT)	U (m s^{-1})	Duration (h)	Channel
1	22 Oct. 1992	9:45	6.0	0.17	1 (lab.)
2	22 Oct. 1992	9:45	6.0	0.17	2 (lab.)
3	22 Oct. 1992	9:45	6.0	0.17	3 (lab.)
4	17 Sept. 1991	10:00	10.0	3.5	
5	25 Nov. 1991	05:00	10.0	2.0	
6	7 Jan. 1991	00:30	20.0	2.5	

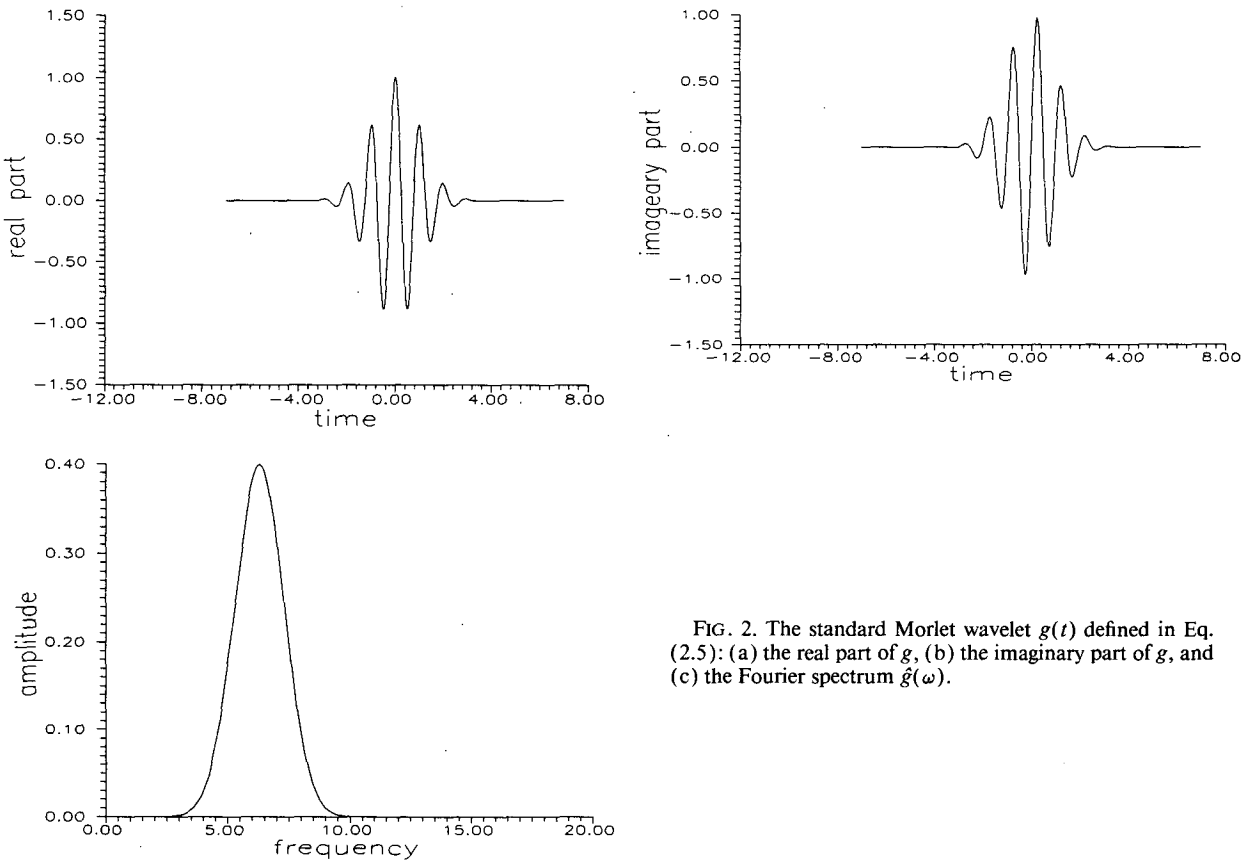

FIG. 2. The standard Morlet wavelet $g(t)$ defined in Eq. (2.5): (a) the real part of g, (b) the imaginary part of g, and (c) the Fourier spectrum $\hat{g}(\omega)$.

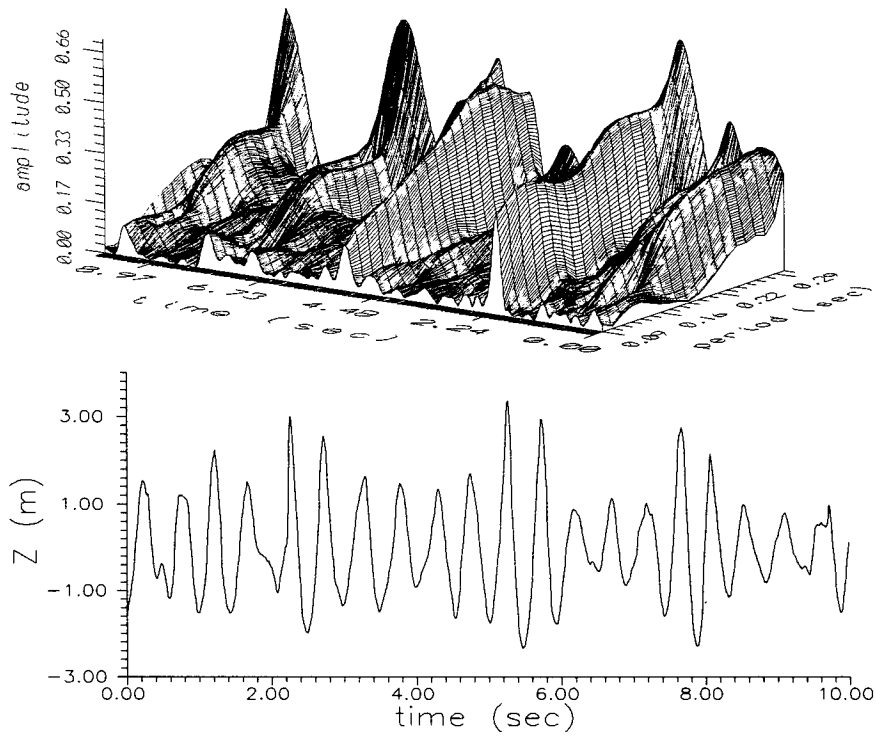

FIG. 3. The wavelet transform of laboratory dataset 2. (a) Three-dimensional display of the modulus $A(\tau, T)$ [with $\tilde{\zeta}(\tau, T) \equiv A(\tau, T)e^{i\phi(\tau,T)}$], the period of the dominant waves being about 4.5 s; (b) the corresponding wave elevation $\zeta(t)$.

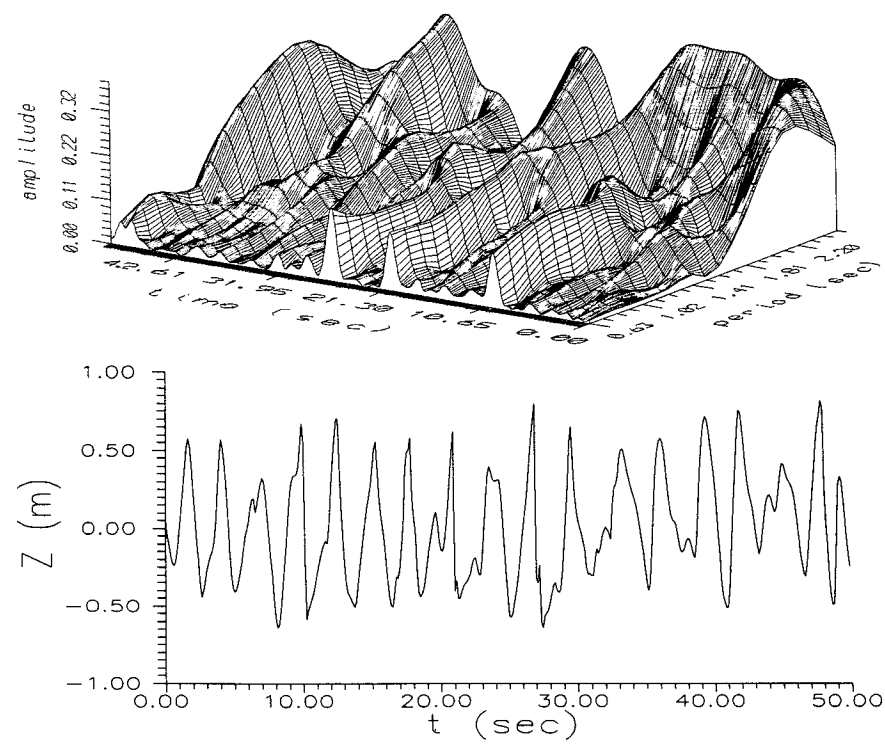

FIG. 4. The wavelet transform of field dataset 4. (a) Three-dimensional display of the modulus $A(\tau, T)$ [with $\tilde{\zeta}(\tau, T) \equiv A(\tau, T)e^{i\phi(\tau,T)}$], the period of the dominant waves being about 2.5 s; (b) the corresponding wave elevation $\zeta(t)$.

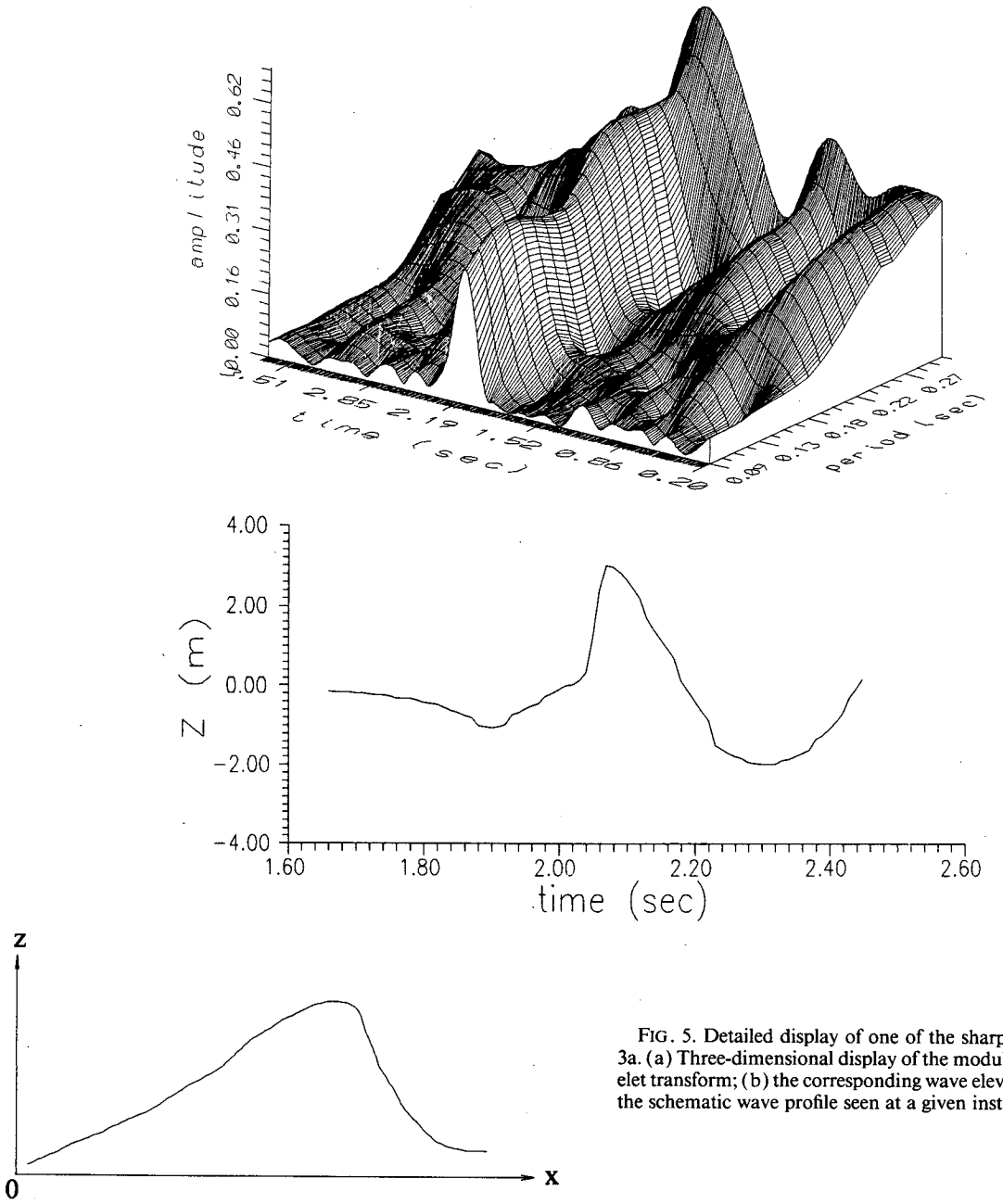

FIG. 5. Detailed display of one of the sharp peaks in Fig. 3a. (a) Three-dimensional display of the modulus of the wavelet transform; (b) the corresponding wave elevation $\zeta(t)$; (c) the schematic wave profile seen at a given instant.

with $\omega_0 = 2\pi/T_0$. The effective width of the wavelet is proportional to the frequency to be analyzed, and they are of the same order. However, for a signal appearing as a group, $\Delta\omega$ should be much less than the principle frequency ω_0. Hence Figs. 3a and 4a imply that the wave components of high frequencies in observed wind wave datasets are not constant in amplitude and that there are sharp peaks sporadically distributed along the time axis. In other words, the high-frequency wave components in wind waves are intermittent. This observation is in contradiction to the wind wave spectral model of Longuet-Higgins Eq. (1.1). According to this model, every wave component should be of constant amplitude.

To decode the origin of the sharp peaked amplitudes of the high-frequency wave components, one of the sharp peaks in Fig. 3a is magnified in Fig. 5a. Let t_0 be the location of the sharp peak in the time axis; then we find that $|\tilde{\zeta}(t_0, T)|$ has the appearance of a power law function of T when T is small. According to the wavelet transform property specified by Eqs. (2.10), (2.11), and (2.12), we assert that this sharp peak is

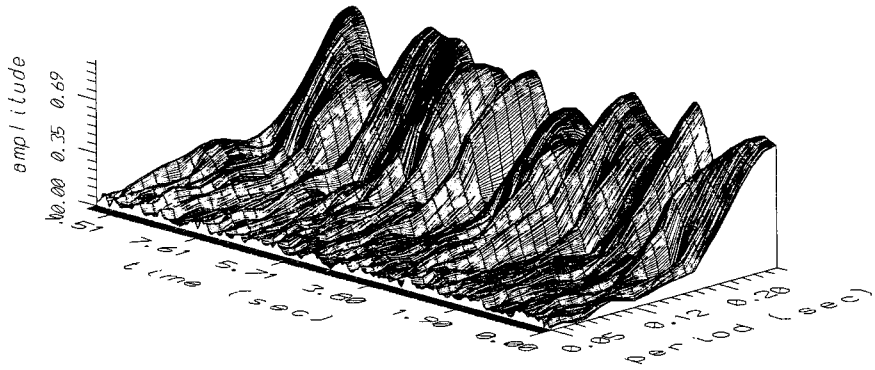

FIG. 6. Three-dimensional display of the modulus of the wavelet transform of laboratory dataset 1, the period of the dominant waves being about 0.24 s.

originated from the singularity specified by Eq. (2.12) in the wind wave datasets being analyzed. The curve in Fig. 5b is the amplification of the original $\zeta(t)$ corresponding to the sharp peak. Ahead of the wave apex the curve is concave, while behind the apex the curve is convex. Schematically, we draw this wave (seen at a given instant) in Fig. 5c. It suggests that the sharp peaks in wavelet space correspond to wave singularities resulting from nonlinear advection, where wave breaking generally occurs.

The influence of wave breaking on the surface pressure distribution in wind–wave interactions was investigated by Banner (1990). It is observed that since the airflow is always separated in the trough between breaking crests, a strong local momentum (and energy) flux to the water surface must appear downwind of the breaking wave trough. Banner's observation is confirmed by the appearance of a sharp peak in the wavelet space coexisting with the horizontal asymmetry of the wave profile resulted from wave breaking.

It is worthwhile to remark that wind waves in nature are always coexisting with different scale water motions involving different physical factors. The horizontal asymmetry of the wave profile may well be produced by nonlinear interaction between the wind waves and other kinds of water motions (see Phillips 1977, section 3.7). It is therefore reasonable to anticipate that this kind of nonlinear interaction may be derived from the wind wave data since it produces local significant enhancement of the energy of short wind wave components. Is it the basic mechanism involved in that internal waves and fronts can sometimes be found from the ocean wave imaging by the synthetic aperture radar technique?

In Figs. 3a and 4a, along the time axis for a given T (T being small), the wave components inside the sharp peaks are dynamically different from the one outside the sharp peaks. Generally, the latter are considered as a free infinitesimal wave component, which satisfies the linear dispersion relation $\omega^2 = gk$, and its group speed is much less than the group speed of the dominant wave component. But the waves inside the sharp peaks, being produced by strongly nonlinear advection, propagate at the same speed as the dominant waves, and there is no effective dispersion among wave components of different scales.

It is expected that breaking of the dominant waves is less active at short fetches. Figure 6 shows the modulus of the wavelet coefficients calculated from laboratory dataset 1, which is observed at a much shorter fetch than that of dataset 2. In this figure there are no sharp peaks at the high-frequency range. It implies that nonlinear advection is not strong enough to cause effective horizontal asymmetry of the wave profiles as shown in Fig. 5c.

To visualize the intermittency of the wave components in the wavelet space, we define the energy intermittency measure (see Farge 1992):

$$I(\tau, T) = \frac{|\tilde{\zeta}(\tau, T)|^2}{\langle |\tilde{\zeta}(\tau, T)|^2 \rangle_\tau} \tag{3.2}$$

with

$$\langle |\tilde{\zeta}(\tau, T)|^2 \rangle_\tau = \lim_{A \to \infty} \frac{1}{A} \int_0^A |\tilde{\zeta}(\tau, T)|^2 d\tau, \tag{3.3}$$

$I(\tau, T) = 1$, $\forall\tau$ and $\forall T$, means that there is no wave intermittency, that is, that each location has the same energy spectrum, which then corresponds to the Fourier frequency spectrum.

Figures 7 and 8 show the energy intermittency measure calculated from laboratory dataset 3 and from field dataset 5. We can see that the wave energy at small scales is highly intermittent in space. In fact, the average of the wavelet coefficients along the τ axis corresponds to the square root of the Fourier frequency spectrum $\sqrt{S(\omega)}$. It can be seen from Figs. 7 and 8 that in the high-frequency range [i.e., the equilibrium range, see Phillips (1985)] the Fourier frequency spectrum is derived from, in a large ratio (being about 60% in these two cases), the noninfinitesimal waves produced with the nonlinear advection mentioned above. This new

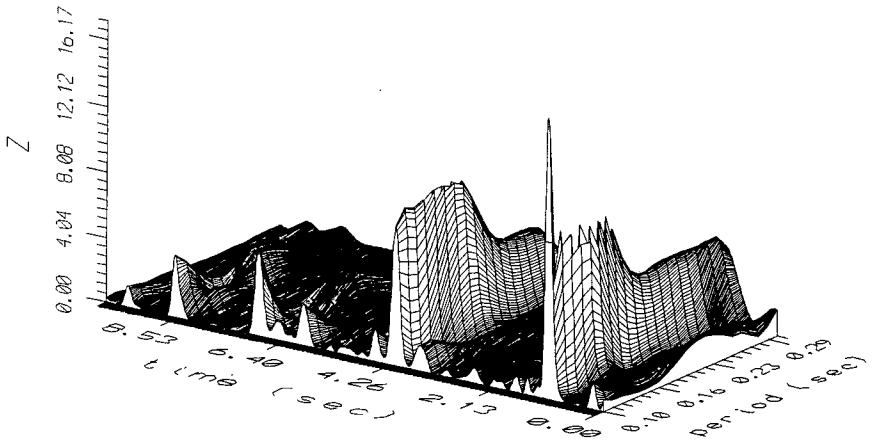

FIG. 7a. The energy intermittency measure $I(\tau, T)$ calculated from the laboratory dataset 3: three-dimensional display of $I(\tau, T)$.

result is important in that it challenges our conventional understanding of wind waves determined by a Fourier frequency spectrum. In this case, the wave components in the equilibrium range estimated from the Fourier frequency spectrum are not effectively the infinitesimal waves satisfying the dispersion relation $\omega^2 = gk$. It is worthy of note that $\omega^2 = gk$ is the essential condition to describe the dynamics of the wind waves by the action conservation law Eq. (1.5), in which each part of the wave components is considered as a wave group traveling at group velocity

$$\vec{C}_g = \mathbf{v}_k \omega. \tag{3.4}$$

It is clear that while the nonlinear advection of dominant waves is active, the mathematical description of Eqs. (1.1), (1.2), and (1.5) will not be convenient for small-scale waves in the equilibrium range.

The dynamics of the averaged properties of short wave components in the equilibrium range was formulated by Phillips in 1958 and 1985, and recent investigation on this subject can be found, for example, in the work of Banner (1989, 1990) and Shen and Mei (1993). Their models, being based on the wave action conservation law Eq. (1.5), are only applicable in regions corresponding to the part outside the sharp peaks in the wavelet space. It is interesting to remark that since the experimental investigation of Banner (1989) was performed on a small square (1.6 m × 1.6 m) of sea surface by a stereophotogrammetric technique, the dominant wave elevations have been automatically filtered out by the applied technique itself. Hence, his wavenumber spectra, having not been biased by the local singularities mentioned above, are effectively in agreement with the predicted spectrum of Phillips (1985); see Shen and Mei (1993). Unfortunately, until now almost all other experimental research on the spectral forms in the equilibrium range has been performed on wind wave datasets of long duration and/or large areas. Because the properties of the dominant wave breaking may well be dependent not only on the wind speed but also on other physical factors, such as the fetch, the stability of the air and water, the water undercurrents, and so on, the local enhancement of

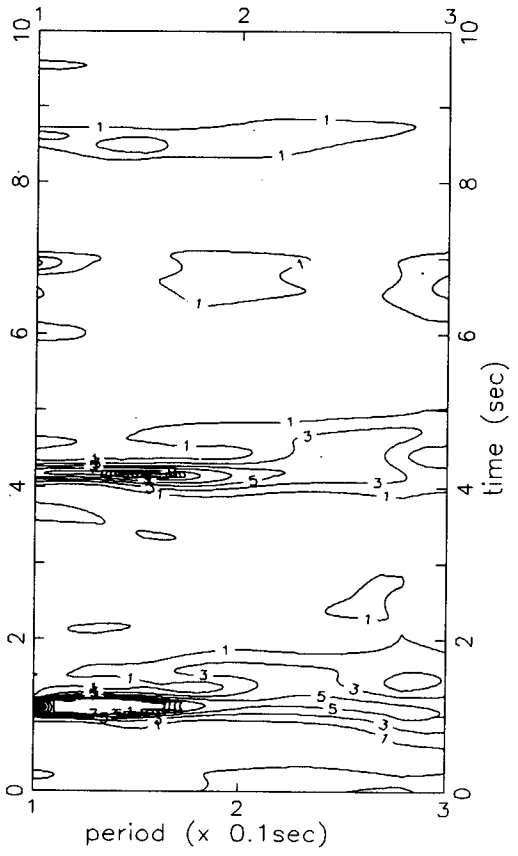

FIG. 7b. The isogram of $I(\tau, T)$.

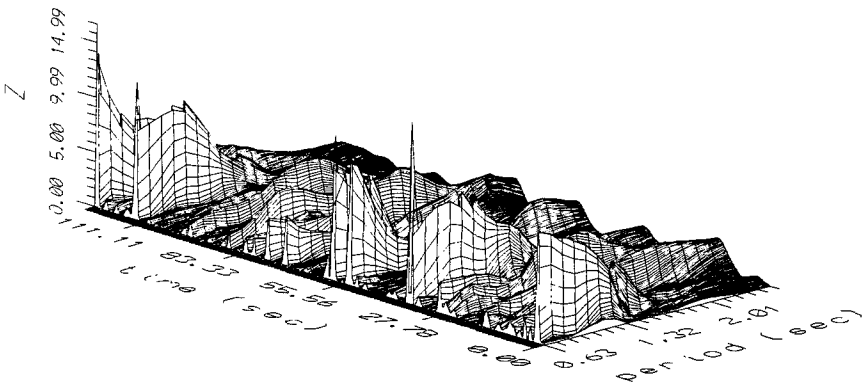

FIG. 8a. The energy intermittency measure $I(\tau, T)$ calculated from field dataset 5: three-dimensional display of $I(\tau, T)$.

short wave components originated from wave breaking should be effectively different between different observations. The consequence is that the observed wind wave spectra in the equilibrium range will manifest considerable fluctuations, as having been observed by Phillips (1985).

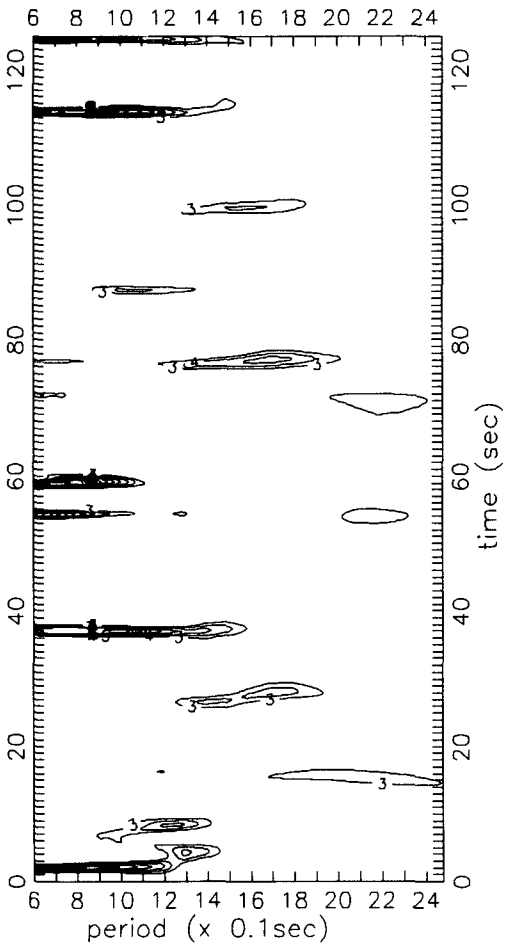

FIG. 8b. The isogram of $I(\tau, T)$.

4. Conclusions

The following conclusions can be drawn from the present study.

1) When one is interested in the short Fourier wave components, the wind wave field must be divided into two classes according to the local property of the short wave components. In the first class, Σ_0 say, the short wave components are effectively infinitesimal and satisfy the linear dispersion relation $\omega^2 = gk$, and the second class, Σ_s say, is characterized by a much enhanced energy density, where the short Fourier wave components are not infinitesimal and propagate without dispersion at the same velocity as the dominant waves.

2) The measure of Σ_s is much less than that of Σ_0, and Σ_s is composed by subsets sporadically distributed on the whole wind-wave field. The ratio of the short wave energy distributed on Σ_s to that on the whole field $\Sigma_0 + \Sigma_s$ can be greater than 50% when the fetch is not too short.

3) The enhancement of the energy of short wave components on Σ_s is physically originated from the horizontal asymmetry of the dominant wave profile shown in Fig. 5c, where the dominant wave is breaking.

4) The equilibrium spectra predicted by Phillips (1985) are only applicable to describe the average properties of the short wave components on Σ_0. More theoretical and experimental investigation of the enhanced short waves on Σ_s should be performed in the future to complete our understanding of the mechanisms of the wind-generated gravity waves.

5) When the fetch is not too short, the action conservation law Eq. (1.5) is not convenient to describe the dynamics of the short wind wave components in the equilibrium range.

Acknowledgments. The authors thank the two reviewers whose thoughtful comments resulted in major improvements to the initial version of this paper. This work was supported both by the National Science Foundation of China and by the State Commission of Education of China. The authors gratefully acknowledge their support.

REFERENCES

Banner, M. L., 1990a: The influence of wave breaking on the surface pressure distribution in wind–wave interactions. *J. Fluid Mech.*, **211,** 463–495.

——, 1990b: Equilibrium spectra of wind waves. *J. Phys. Oceanogr.*, **20,** 966–984.

——, I. S. F. Jones, and J. C. Trinder, 1989: Wavenumber spectra of short gravity waves. *J. Fluid Mech.*, **198,** 321–344.

Farge, M., 1992: Wavelet transforms and their applications to turbulence. *Annu. Rev. Fluid Mech.*, **24,** 395–457.

Goupillaud, P., A. Grossmann, and J. Morlet, 1984: Cycle-octave and related transforms in seismic signal analysis. *Geoexploration,* **23,** 85–105.

Grossmann, A., and J. Morlet, 1987: *Decomposition of Functions into Wavelets of Constant Shape and Related Transforms.* World Scientific.

Khandekar, M. L., 1989: *Operational Analysis and Prediction of Ocean Wind Waves.* Springer-Verlag.

Kitaigorodskii, S. A., 1983: On the equilibrium range in the spectrum of wind-generated gravity waves. *J. Phys. Oceanogr.*, **13,** 816–827.

Longuet-Higgins, M. S., 1957: The statistical analysis of a random moving surface. *Phil. Trans. Roy. Soc. London,* **A249,** 321–387.

Phillips, O. M., 1958: The equilibrium range in the spectrum of wind-generated ocean waves. *J. Fluid Mech.*, **4,** 426–434.

——, 1977: *The Dynamics of the Upper Ocean.* Cambridge University Press.

——, 1985: Spectral and statistical properties of the equilibrium range in wind-generated gravity waves. *J. Fluid Mech.*, **156,** 505–531.

Shen, Z., and L. M. Mei, 1993: Equilibrium spectra of water waves forced by intermittent wind turbulence. *J. Phys. Oceanogr.*, **23,** 2019–2026.